Algorithms for Automatically Pointing Ultrasound Imaging Catheters

Paul M. Loschak, *Student Member, IEEE*, Laura J. Brattain, *Member, IEEE*, and Robert D. Howe, *Fellow, IEEE*

Abstract—A system for automatically pointing ultrasound (US) imaging catheters will enable clinicians to monitor anatomical structures and track instruments during interventional procedures. Off-the-shelf US catheters provide high-quality US images from within the patient. While this method of imaging has been proven to be effective for guiding many interventional treatments, significant training is required to overcome the difficulty in manually steering the imager to point at desired structures. Our system uses closed-form four degree-of-freedom (DOF) kinematic solutions to automatically position the US catheter and point the imager. Algorithms for steering and imager pointing were developed for a range of useful diagnostic and interventional motions. The system was validated on a robotic test bed by steering the catheter within a water environment containing phantom objects. While the system described here was designed for pointing US catheters, these algorithms are applicable to accurate 4-DOF steering and orientation control of any long thin tendon-driven tool with single or bidirectional bending.

Index Terms—Flexible manipulators, surgical robotics, ultrasound (US) imaging.

I. INTRODUCTION

TECHNOLOGICAL advances in medicine have aimed to reduce the invasiveness of surgery and catheters are becoming more popular for performing minimally invasive cardiac procedures. Intracardiac echocardiography (ICE) uses an ultrasound (US) array transducer in the tip of a steerable catheter to transmit side-facing images of soft tissue structures in real time. US catheters can increase the safety and effectiveness of procedures while being minimally-invasive, portable, and cost effective. However, its use is limited because steering the imaging plane is highly challenging and requires significant training to master. The difficulty in navigating US catheters has limited its use to critical phases of procedures, such as performing transseptal punctures, in which the safety benefits of using US catheters have been proven to offset the cost and difficulty required to use them [1], [2]. Therefore, we aim to

Fig. 1. Diagram of system pointing US imager in the heart.

develop a system for automatic pointing of US imaging catheters (see Fig. 1).

The proposed system provides different functionality than current commercial catheter robots. These systems [3]–[9] enable teleoperation of catheter controls to increase operator comfort and reduce exposure to radiation from fluoroscopic imaging. Some of these systems can be used with ICE catheters, but most systems are interfaced in control knob joint space, which does not mitigate the difficulties of aiming imaging catheters using direct manual control. Existing systems controlled in Cartesian coordinates do not feature orientation control.

Previous conference and workshop papers on automatically steering US catheters introduced the four degree-of-freedom (DOF) control problem and presented preliminary positioning and imager steering results [10], [11]. A limited subset of navigational capabilities for position control and imager rotation was demonstrated. Imager rotation for instrument tracking and imager three-dimensional (3-D) positioning have since been expanded to more general cases. Position and orientation steering accuracies for all test cases have since been improved as well.

This paper provides an expanded in-depth analysis on the 4-DOF catheter steering system to enable new diagnostic and treatment capabilities. A model relates catheter control actions with catheter tip locations and US imaging plane orientations. Algorithms for visualization strategies for specific tasks were created in conjunction with the bending model. The model was validated with a 4-DOF robot by automatically navigating the US catheter to a desired pose and pointing the imager at desired targets. This paper aims to help clinicians achieve the needed views during procedures while reducing patient and staff exposure to radiation.

This article has been accepted for inclusion in a future issue of this journal. Content is final as presented, with the exception of pagination.

2

IEEE TRANSACTIONS ON ROBOTICS
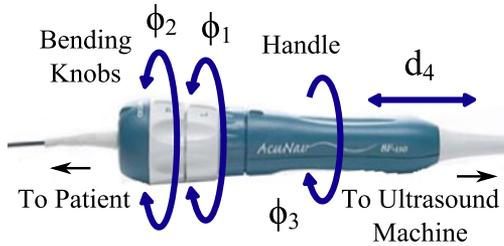
Fig. 2. Handle of the AcuNav US imaging catheter showing control DOFs.

II. BACKGROUND

A. US Catheters

US catheters are steerable devices that acquire US images of adjacent tissues from the distal tip. They can be guided through the vasculature to various organ systems, such as the inside of the heart, where they can provide views of fast moving heart structures with resolution that may not be possible with external probes. US catheters can also be used for continuous monitoring of radiofrequency (RF) energy delivery during cardiac ablations.

The catheter consists of a plastic handle that can be rotated about or translated along its axis. Four pull wires (spaced $90°$ apart in cross section) extend along the length of the catheter body through the bending section to their attachment points at the distal tip. At the distal end, the bending section is designed to be less rigid than the body such that pull wire deflection causes most bending to occur in the bending section. On the proximal end, each pair of opposing pull wires connects to a bending knob.

Steering is done by rotating two knobs (pitch and yaw), rotating the handle of the catheter (roll), and translating the handle. The distal 2 cm tip of the catheter is rigid and contains the US transducer. The US catheter used for system validation was a 10 Fr (3.30 mm diameter) 110 cm long catheter with a 64-element 2-D US transducer at its distal tip (AcuNav, Biosense Webster, USA). AcuNav is the most common side-facing US catheter in clinical use at present. The catheter handle with joint inputs is labeled in Fig. 2. The resulting tip motions are diagrammed in Fig. 3.

B. Existing Kinematics

Kinematic calculations for the robotic positioning of long thin flexible manipulators have been examined through many strategies. Material mechanics models [12], geometrically-derived analytical models [13], [14], Denavit–Hartenberg parameter-based models [15], remotely actuated continuum models [16], [17], and model-less approaches [18] have been developed by previous researchers. Catheter orientation calculations have been described in previous work [19], but control of catheter tip orientation has not yet become a focus of investigation. We will use geometrically-derived analytical models as the basis of our approach to control the 3-DOF position and 1-DOF of orientation for the US catheter.
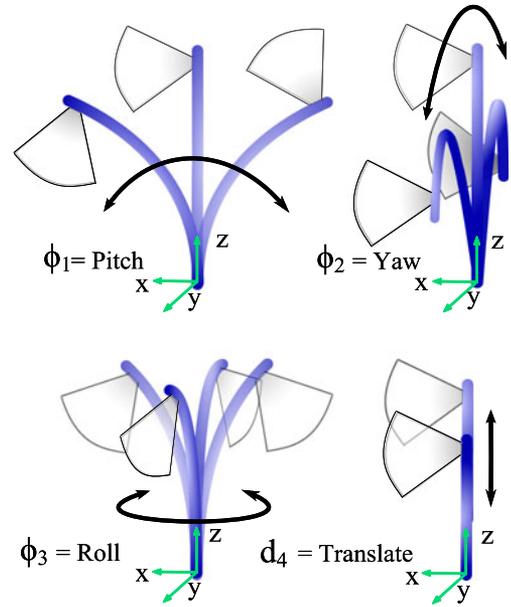
Fig. 3. Corresponding tip motion directions.

III. ALGORITHM DESIGN

A. Kinematics Strategy

A commercial AcuNav ICE catheter (Biosense Webster, USA) has four actuated DOF. Our system actuates the 4 DOF that are used in manual manipulation: pitch bending knob, yaw bending knob, catheter handle roll, and catheter handle translation. Typical cardiac catheters for tissue interaction (i.e., ablation catheters) reach desired positions with 3 DOF: one plane of bending, handle roll, and handle translation. US catheters use an extra bending direction to reach desired tip orientations for imaging. Kinematic calculations and robotic control enable utilization of the 4 DOF in different ways depending on the desired visualization.

The kinematics presented here and in previous work [10] model the relationship between the joint space control knobs and the task space US imager pose. The kinematic model was based on geometric principles and classic robot kinematics. Closed-form kinematic solutions have been derived for both the forward and inverse cases. This model is unique in that it is the first model known to the authors to be applied toward controlling both the position and orientation of the tip for catheters with two bending directions. With orientation information, it is then possible to determine the location and direction of the US image.

A primary assumption of the model is that catheter bending occurs in the bending plane (neglecting the effects of plastic torsion). A second assumption of the model specifies that the base of the distal bending section is constrained to allow free rotation but maintain a fixed distance from the catheter handle. The fixed base enables the kinematic model to assume that joint-level inputs are conveyed directly to the distal bending section of the catheter without nonlinear losses throughout the catheter body. We also assume that the catheter bends with a constant radius of curvature, which has been examined previously [16], and that

This article has been accepted for inclusion in a future issue of this journal. Content is final as presented, with the exception of pagination.

LOSCHAK *et al.*: ALGORITHMS FOR AUTOMATICALLY POINTING ULTRASOUND IMAGING CATHETERS

3
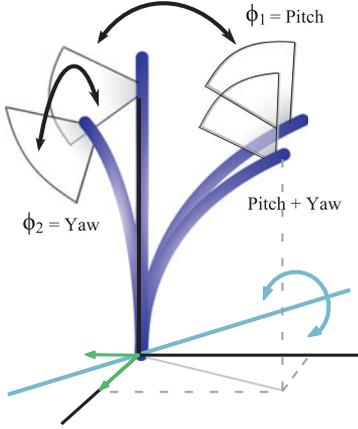
Fig. 4. Pitch and yaw of this parallel continuum manipulator are decoupled in position control.

Fig. 5. (a) Catheter bending geometry, (b) inverse kinematics.

dynamic effects of catheter motion are negligible due to low-speed actuation. Physiological motions such as heartbeat and blood flow will further reduce system accuracy in live patients, but such effects are not yet examined in this benchtop work.

An additional assumption for deriving the kinematic solution to the system involves positional joint coupling in bidirectional bending. Solving for the tip orientation of a traditional serial manipulator would normally require multiplying the origin orientation by transformation matrices corresponding to each joint's orientation change in the proper order (depending on the manipulator). However, the bidirectional bending catheter is a manipulator in which pitch and yaw can occur simultaneously. We begin by making the assumption that the effects of positional coupling between bending directions are negligible. It is assumed that applying pitch then yaw will yield the same kinematic results as applying yaw then pitch (see Fig. 4). The orientation of the bent catheter can be calculated by rotating about an axis (see Fig. 4 blue line), which represents the ratio of yaw to pitch input to the system. This claim was validated in [10].

B. Forward Kinematics

The forward kinematics model uses the catheter handle inputs to calculate the position and orientation at the catheter tip. The catheter handle inputs correspond to the four controllable actuated DOFs as in Fig. 3. The first input bending knob controls yaw in the right-left plane, ϕ_1, the second input bending knob controls pitch in the posterior–anterior plane, ϕ_2, the third input is catheter handle rotation (roll), ϕ_3, and the fourth input is catheter handle translation, d_4. The constants for catheter radius, R_c, length of bending section, L, and effective knob diameter, D_K, must be known as well. Intermediate variables [see Fig. 5(a)] are useful to describe the bending of the distal section [13]. The ratio of yaw to pitch

$$\theta = \tan^{-1}\left(\frac{\phi_1}{\phi_2}\right) \tag{1}$$

is the angle between the bending plane and the $X - Z$ plane. The amount of pitch and yaw pull wire deflections due to the
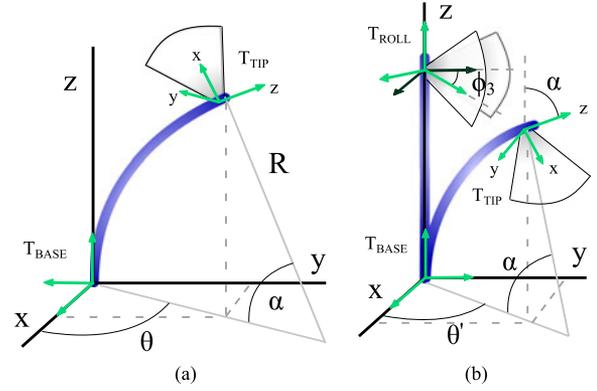
bending knobs are ΔL_1 and ΔL_2, where

$$\Delta L_1 = \phi_1 \frac{D_K}{2}, \quad \Delta L_2 = \phi_2 \frac{D_K}{2}. \tag{2}$$

Curvature can be described by the angle

$$\alpha = \sqrt{\left(\frac{\Delta L_1}{R_c}\right)^2 + \left(\frac{\Delta L_2}{R_c}\right)^2} \tag{3}$$

and the radius of curvature is

$$R = \frac{L}{\alpha}. \tag{4}$$

The catheter tip position from bending can be calculated in terms of R, α, and θ as

$$X = R\left(1 - \cos\alpha\right)\cos\theta \tag{5}$$

$$Y = R\left(1 - \cos\alpha\right)\sin\theta \tag{6}$$

$$Z = R\sin\alpha. \tag{7}$$

It should be noted here that θ and Z are dependent only on adjustments in the bending knobs (and not handle rotation or translation). Handle rotation and translation will be applied in a later step.

The tip orientation due to bending can be calculated by the equivalent axis theorem

$$R_{\text{TILT}}(\alpha, \mathbf{u}) =$$
$$\begin{bmatrix} u_1^2 V_\alpha + C_\alpha & u_1 u_2 V_\alpha - u_3 S_\alpha & u_1 u_3 V_\alpha + u_2 S_\alpha \\ u_1 u_2 V_\alpha + u_3 S_\alpha & u_2^2 V_\alpha + C_\alpha & u_2 u_3 V_\alpha - u_1 S_\alpha \\ u_1 u_3 V_\alpha - u_2 S_\alpha & u_2 u_3 V_\alpha + u_1 S_\alpha & u_3^2 V_\alpha + C_\alpha \end{bmatrix} \tag{8}$$

which states that any orientation change can be expressed as a rotation about a fixed axis [20]. This rotates the orientation by angle α about a new axis $\mathbf{u}$ that is orthogonal to the bending plane (see Fig. 4 blue line). Here $C_\alpha = \cos\alpha$, $S_\alpha = \sin\alpha$, and $V = (1 - \cos\alpha)$. The unit vector $\mathbf{u}$ is calculated by cross products of vectors relating the catheter tip to the base of the bending section and the center of the bending arc. A 4×4 transformation matrix, $T_{\text{TILT}}(\phi_1, \phi_2, u)$, is then assembled to tilt the bending tip with respect to the bending base. This contains (8) as the rotation and values from (5)–(7) as tip position. Next, the handle rotation and translation matrices, $T_{\text{ROLL}}(\phi_3)$ and $T_{\text{TRANS}}(d_4)$,

are premultiplied to calculate the final position and orientation

$$T_{\text{TIP}} = T_{\text{TRANS}}(d_4) T_{\text{ROLL}}(\phi_3) T_{\text{TILT}}(\phi_1, \phi_2, \mathbf{u}). \quad (9)$$

C. Inverse Kinematics

The inverse kinematic model uses (9) as input and solves for the single possible catheter configuration. While there are several strategies to calculate the inverse kinematics, this strategy was chosen such that the imager could be specified to point in the proper plane. The z-axis of the orientation at the catheter tip is assumed to be tangent to the catheter arc. Therefore, it is possible to solve for intermediate variables α and R which describe the bending in Fig. 5(b). Calculating the dot product of the world z-axis and the catheter tip z-axis defines the tilt

$$\alpha = \cos^{-1}\left(\mathbf{z}^0 \cdot \mathbf{z}^{\text{TIP}}\right). \quad (10)$$

Now we must analyze rotation, but it is currently not possible to identify whether the bending planes rotation occurred due to bending θ, handle roll ϕ_3, or a combination of both. Therefore in the meantime, we can use the x and y values of the catheter tip to solve for a nominal angle value

$$\theta' = \tan^{-1}\left(\frac{y}{x}\right) \quad (11)$$

which will be used to calculate the true θ. Equation (8) may be applied once again to rotate the tip orientation by α about an axis orthogonal to the bending plane. The orthogonal axis $\mathbf{u}'$ is used to find the true value. Applying (8) results in transforming the tip orientation to an intermediate orientation in which the new z-axis is collinear with the world frame z-axis. The resulting angle between the nominal x-axis and the world frame x-axis is the handle rotation angle, ϕ_3. In this way, we have systematically "reversed" the bending to reveal the inputs that will allow the catheter to achieve the desired configuration. With ϕ_3, we may calculate the true θ and the pull wire displacements as

$$\Delta L_1 = R_c \alpha \sqrt{1 + \tan^2\theta} \quad (12)$$
$$\Delta L_2 = -R_c \alpha \tan\theta \sqrt{1 + \tan^2\theta} \quad (13)$$
$$d_4 = Z_{\text{TIP}} - R\sin\alpha. \quad (14)$$

With all four catheter inputs known, converting the values to actuator space becomes trivial. The inverse kinematic function allows the system to use the catheter's desired position and orientation and calculate the required motor commands. Position control (without orientation information) can be achieved with minimal calculation by (1)–(7) to solve for ϕ_1, ϕ_2, and d_4.

D. Imager Spinning

The bidirectional bending catheter is a 4-DOF system which can be position controlled to any point in the workspace by using 3 DOF. The extra DOF can then be used to orient the imaging plane in any direction that is orthogonal to the tip of the catheter. This provides safe imaging because the US plane can be rotated about the axis of the catheter tip while the ICE catheter is fixed to the same location. Fig. 6 demonstrates the process of navigating the catheter to the same position in space using two different steering methods: yaw combined with roll
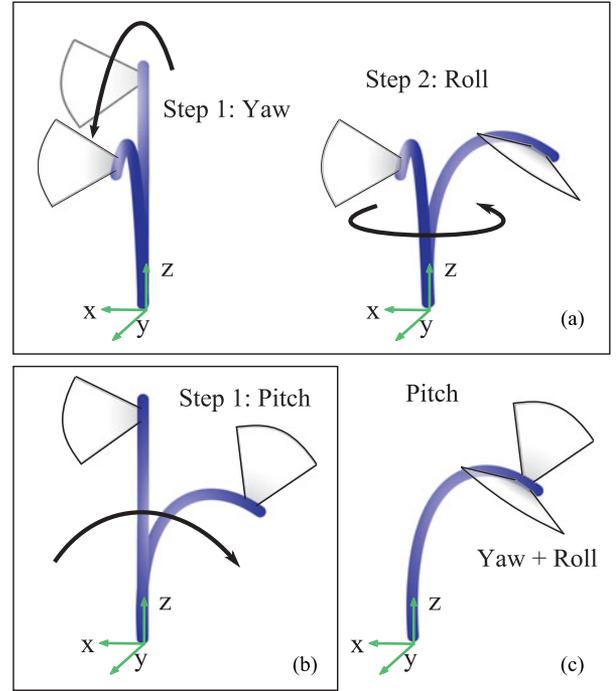
Fig. 6. (a) Yaw and roll are applied to the catheter. (b) Pitch is applied to the catheter. (c) Two cases are overlaid demonstrating that the catheter may be position controlled to the same location with varying orientations.

or only pitch. The US imager points in a different direction depending on which steering strategy is used. In Fig. 6(a), the catheter begins with the imager pointed to the left. It is first bent in yaw to reach a new position while the imager remains pointed to the left. The catheter is then rolled by 90° about the base to point the imager out of the plane toward the reader. In Fig. 6(b), an identical catheter in the original position is bent in pitch causing the imager to point upward. In Fig. 6(c), the two navigation strategies are overlaid. For each position, there exists a solution set of specific combinations of pitch, yaw, and roll adjustments that reach the same position in space with a different orientation to aim the imager in a different direction. In practice, this means that the imager may be rotated in 1 DOF about the tip of the catheter without displacing the catheter tip by carefully manipulating the three joints simultaneously (see Fig. 7). This technique enables the robot system to spin the US imager across regions of tissue while collecting images. Coordinating motion between the three joints is extremely difficult to manually accomplish.

The desired US imager spin by angle ψ is applied to the tip's mobile z-axis coordinate frame

$$T_{\text{SPIN}} = \begin{bmatrix} \cos\psi & -\sin\psi & 0 & 0 \\ \sin\psi & \cos\psi & 0 & 0 \\ 0 & 0 & 1 & 0 \\ 0 & 0 & 0 & 1 \end{bmatrix} \quad (15)$$

$$T_{\text{NEW}} = T_{\text{TIP}} T_{\text{SPIN}} \quad (16)$$

which calculates the new catheter pose. The controller (described in Section IV) then rotates the imager while maintaining the fixed position of the catheter tip.

This article has been accepted for inclusion in a future issue of this journal. Content is final as presented, with the exception of pagination.

LOSCHAK *et al.*: ALGORITHMS FOR AUTOMATICALLY POINTING ULTRASOUND IMAGING CATHETERS 5
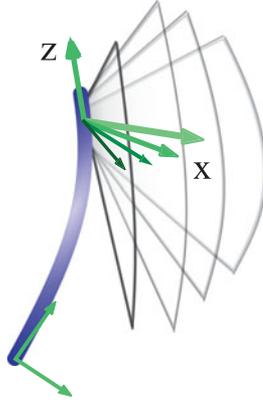
Fig. 7. Imager spinning from fixed catheter location.
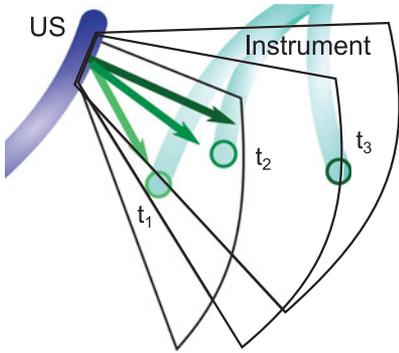
Fig. 8. Schematic of US imager tracking catheter instrument tooltip. Tooltip is navigated to three sequential locations (t_1, t_2, t_3) within the US catheter imaging workspace.

E. Instrument Tracking

The system tracks an instrument tooltip (e.g., ablation catheter) by keeping the tooltip consistently within the US imaging plane. This assumes that the tooltip location is known (in this case, by EM tracker). Fig. 8 demonstrates an ablation catheter being manually moved by the clinician to three different locations. The green arrows represent vectors within the imaging plane, where the imaging plane is continuously adjusted to point directly at the tooltip target while keeping its tip at a fixed and safe location. We achieve this by computing the angle between the target and the US imaging plane and then using (16). The controller (described in Section IV) maintains the position of the catheter tip. It is assumed that the tooltip is manually positioned within the available imaging depth of the US transducer (up to 15 cm) and within the $90°$ wide image angle. If the tooltip is moved outside this range, then the US catheter must be navigated to a new position in order to continue visualizing the tooltip.

F. Imager 3-D Positioning

In the previous sections, a method for imager rotation was described in which a desired angular change is specified while the position must remain constant. In this section, a different imaging technique with an opposite goal is developed. The tip
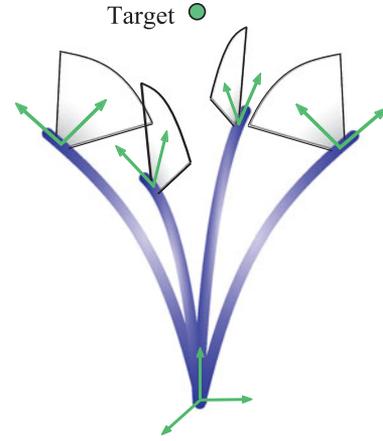
Fig. 9. Example of positions moving the catheter around a target while aiming the imager at the target.

of the US catheter can be rotated around a stationary target while maintaining US imager alignment focused on that target. The US catheter is made to rotate in a circle around a point in space at a constant focal distance F_D, away from the point. Fig. 9 shows a simulation of this motion. For each F_D and object location (within the workspace), there is a solution set of potential catheter positions that will enable the imager to continue pointing at the object. The solution set exists at the intersection of the sphere created by the focal distance and a chordal plane through that sphere. The direction of the chordal plane depends on required catheter curvatures for pointing the imager directly at the target. The radius of the chordal plane is related to F_D and L.

The solution set is calculated by first examining the location of the target and identifying the plane of bending which includes the object and the catheter. Within this plane there are two solutions enabling the imager to be F_D away from the target and pointed directly at the target. These two solutions are analogous to the classic robot arm "elbow up, elbow down" case for conventional robot arms. These solutions are calculated by solving for α

$$T_{xyz}(\alpha, \theta) T_{\text{roll}}(\theta) T_{\text{pitch}}(\alpha) T_{\text{US}} T_{\text{FD}} - T_{\text{object}} = 0 \quad (17)$$

where T_{xyz} is transformation due to the catheter bending calculated by (5)–(7), T_{roll} is a function of θ (which is a function of the target location), T_{pitch} is obtained by rotating about the y-axis by α, T_{US} is the constant transform from the tip of the bending region to the center of the US imager (d_{US}), T_{FD} is the constant transform from the US imager to the target along the x-axis, and T_{object} contains the position of the target. Only the target position is used; not orientation. This calculation differs from (9) because yaw is not needed to point the imager directly at the target while the target is in the same plane as catheter bending.

Equation (17) calculates a 4×4 transformation matrix relating the catheter configuration space to the location of the target object. The bending plane is oriented to include the object. The right-hand column of (17) (the 4th column) contains a 3×1
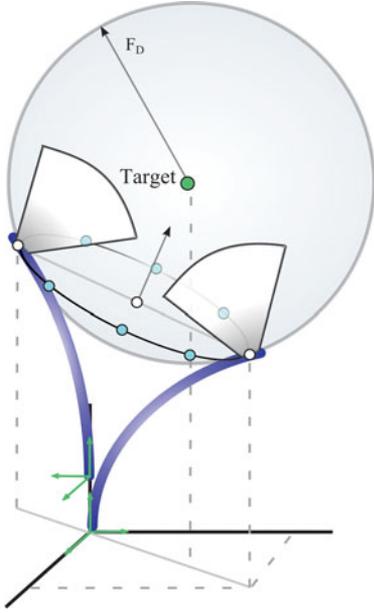
Fig. 10. Solution set geometry.

Fig. 11. US catheter steering robot with 4-DOF.–Dashed outline shows catheter handle location within control actuators.

vector of the catheter tip x, y, and z calculations

$$
\begin{bmatrix}
\dfrac{L}{\alpha}\left(1-c_\alpha\right)c_\theta + d_{\mathrm{US}}c_\theta s_\alpha - F_D\left(s_\theta s_{\mathrm{US}} - c_\theta c_\alpha c_{\mathrm{US}}\right) - O_x \\[4pt]
\dfrac{L}{\alpha}\left(1-c_\alpha\right)s_\theta + d_{\mathrm{US}}s_\theta s_\alpha - F_D\left(c_\theta s_{\mathrm{US}} + s_\theta c_\alpha c_{US}\right) - O_y \\[4pt]
\dfrac{L}{\alpha}s_\alpha + d_{\mathrm{US}}c_\alpha - F_D s_\alpha c_{\mathrm{US}} - O_z
\end{bmatrix}
$$
$$
= 0 \tag{18}
$$

where (O_x, O_y, O_z) refers to the position of the target object. All quantities but α are known. A single-variable nonlinear zero-finding algorithm is used to solve for α in the first and second rows of (18). Positive F_D calculates the elbow up α and negative F_D calculates the elbow down α. Both α values returned are the closest to zero (minimum bending effort) and they will satisfy both the O_x and O_y equations. The third row is then used to solve for the required handle translation. Both α values are input to the forward kinematics to calculate the elbow up/down catheter tip positions, shown in Fig. 10 as white dots. Next, a vector is formed from the midpoint between positions and the target. This is the normal vector of the chordal plane. The solution set of possible locations for positioning the catheter to image the target exists on the circle where this chordal plane intersects the F_D sphere. Equally spaced positions around the circle (denoted by blue dots) were chosen for experimental validation of the calculations.

Each position on the circle represents a point at which the catheter is capable of achieving the proper curvature to point the imager directly at the target and be F_D away from the target. But by simply using the position controller to reach each of these positions, the imager may not necessarily point at the target. A significant amount of imager spinning (up to $\pm 180°$) may be necessary. The roll adjustment can be precalculated through

the kinematics and executed in conjunction with positional navigation. This will roll the catheter first and then position the catheter tip accurately at each desired point around the chordal circle such that minimal imager spinning adjustments at each location are needed.

IV. VALIDATION METHODS

A. Robot

The robot pictured in Fig. 11 was constructed in our previous work to actuate the catheter handle knobs and provide the 4 DOF used in the model [10], [11]. Each DOF was actuated by 6.5 W brushed DC motors driven by digital positioning controllers (EPOS2, Maxon Motor, Switzerland). The actuation strategy was designed for two motors (pitch and yaw bending knobs) to be grounded to the catheter handle, one motor (roll) to be grounded to the linear stage, and one motor (translation) to be grounded to the table. Two bending knob actuators, mounted directly to the catheter handle, were connected to the knobs by timing belts. The ends of the catheter handle were connected to ball bearings allowing rotation about the handle center axis. The roll actuator was connected to the catheter handle by a timing belt. The entire system was mounted to a lead screw driven translation stage. For initial testing, the catheter handle and the distal bending section of the catheter (7 cm) were separated by a fixed distance. A fixture supported the distal bending section while still allowing free rotation about the handle axis.

B. Accuracy Requirements

Controlling the US imager pose involves both the catheter tip sensor accuracy and the US plane properties. The catheter tip pose is measured by 6-DOF electromagnetic (EM) trackers with accuracy rated at 1.4 mm and 0.5° across a 60 cm cube workspace. The clinical settings (electrophysiology suites) and bench top settings are designed to minimize EM interference, and relative pose measurements between nearby sensors are

This article has been accepted for inclusion in a future issue of this journal. Content is final as presented, with the exception of pagination.

LOSCHAK *et al.*: ALGORITHMS FOR AUTOMATICALLY POINTING ULTRASOUND IMAGING CATHETERS

7
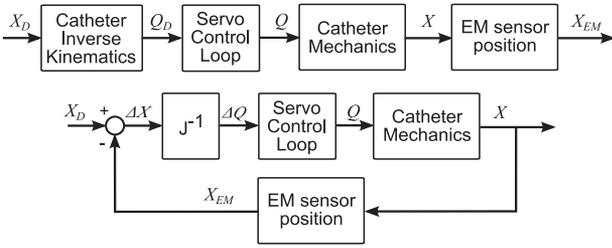
Fig. 12. Position controller (top) inverse kinematics loop for large motions, (bottom) Jacobian loop for small corrections.

Fig. 13. Control diagram for position and imaging angle.

more accurate. The US plane has a thickness that varies by depth from the transducer. A conservative approximation of the US plane thickness is 4 mm. EM tracker errors may result in misalignment of the US plane with the target. For an example scenario of a 3 mm ablation catheter target located 10 cm away from the transducer, the worst EM tracker accuracy will still enable the US imager to intersect with the edge of the target and there will still be additional room for error. Therefore, allowable positioning and orientation errors (typically 2 mm and 0.45°) are programmed into the controller.

C. Position Controller

The system's control strategy is a function of the distance between the catheter tip and the desired tip position. For large motion changes above a specified distance threshold the inverse kinematics calculations use the desired task space position X_D to calculate the joint space solution Q_D [see Fig. 12 (top)]. A low-level control loop drives each actuator to reach the commanded joint angles, Q. The catheter is bent and then an EM sensor on the tip of the catheter measures its position, X_{EM}. Due to uncertainties with polymer effects in continuum robots and inaccuracies in the system, the joint inputs calculated directly from inverse kinematics typically do not position the catheter tip precisely at the desired position. Therefore, an iterative cycle of small position adjustments is used to reach the target precisely.

The error between the current measured position and the target position is then calculated as the desired change in task space coordinates ΔX, which is used in an inverse Jacobian calculation to obtain ΔQ. The Jacobian is obtained by differentiating (5)–(7). The cycle of measurement and adjustment continues as in Fig. 12 (bottom) until the catheter has reached the desired position within a specified threshold.

D. Serial Position and Imager Controller

The control strategy used for imager sweeping and motion around targets is an expansion upon the positioning controller described above. A proportional controller adjusts roll in series with the position controller maintaining the desired position. Although both the imager angle and the catheter position are dependent on roll and pitch/yaw/translation, it will be shown that controlling roll and position in series leads to accurate results. Fig. 13 is a diagram of this strategy. First, the catheter is navigated by position control (see Fig. 12) toward the desired position, X_D. The low-level control, catheter mechanics, and
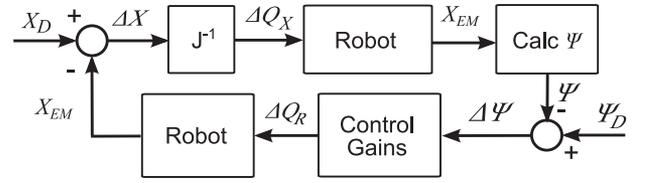
EM sensing steps are summarized as "Robot." Next, the orientation of the catheter tip (contained in X_{EM}) is used to calculate the angle between the image plane and the target, ψ. This angular difference is multiplied by a proportional gain ($K_P < 1$) and the roll actuator rotates the catheter handle by ΔQ_R. Then, the position controller is activated again to ensure that the catheter tip remains at the correct position. Position changes affect ψ (unless the robot performs translation only), which is recalculated and the roll axis is adjusted again.

This loop of position adjustment, angle measurement, roll adjustment, and position measurement continues until both the imager angle and the catheter tip position have reached their desired locations within specified tolerances. The iterative nature of this controller achieves accurate navigation without the need to compensate for the pull wire slack dead zone. Therefore, dead zone compensation is not discussed in this paper. We recognize that this may be a necessary feature in future navigation at higher speeds.

V. EXPERIMENTAL RESULTS

A. Position Steering

The kinematic and control methods described above were used to move the catheter tip to a sequence of specific user-defined locations along a path across the workspace. These experiments focused solely on position control, without regard to the imaging plane directionality. Therefore, only 3 DOF required for positioning (chosen to be pitch, yaw, and translation) were used. Square paths were chosen because this shape requires the robot to adjust all 3 DOFs in navigating to every point. The controller moved the catheter tip toward the desired point until it reached the location (within a tolerance of 2 mm). Then, the robot was commanded to move to the second point, and so on. Shapes in various planes were tested and typical results are shown in Fig. 14. The catheter tip successfully navigated to each position within the specified accuracy threshold distance, resulting in positioning error 1.9 mm rms. The joint space adjustments required for creating this trajectory are shown in Fig. 15, illustrating the difficulty in manually achieving tip control through simultaneous adjustment of three control inputs.

B. Imager Spinning

The imager spinning algorithm was used to adjust the angle of the imaging plane 11 times in user-defined increments of 5° per adjustment. The results of one trial are shown in Fig. 16. The green lines represent the same vector in each imaging plane as the imager is rotated. The color intensity represents the order in which rotations occurred. The lightest green arrow represents
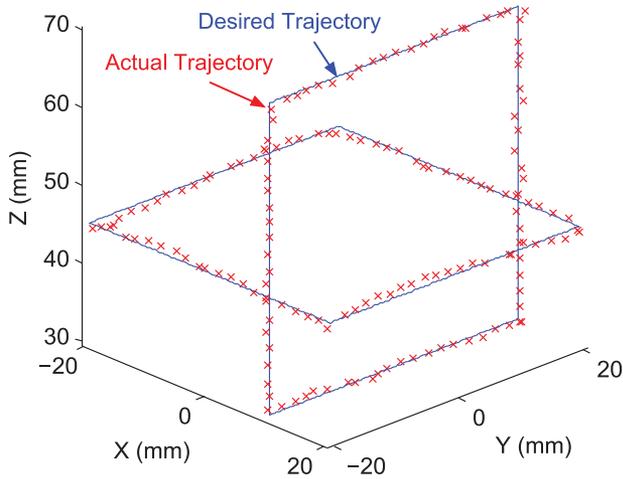
Fig. 14.   Catheter position control experimental results. Lines are commanded positions, symbols are measured positions.

Fig. 16.   Results of sweeping tests. Green lines represent the same vector within each imaging plane as the imager is rotated.

Fig. 15.   (top) Calculated joint adjustments required to navigate the catheter tip in a square trajectory. (middle) Actual joint adjustments required to navigate the catheter tip in a square trajectory. (bottom) *X*-axis catheter tip trajectory.

Fig. 17.   Actual joint adjustments required to rotate the US imager while remaining at a fixed location.

angular adjustment 5° per step resulted in 0.25° rms error and unwanted catheter tip displacement 1.0 mm rms error.

C. Instrument Tracking

The instrument tracking algorithm was tested on a phantom in a water tank environment. The phantom left atrium was made from a gelatin mixture containing powdered fiber supplement to mimic the echogenic properties of live tissue in US imaging [21]. The mixture was molded into the shape of a left atrium with an opening roughly 40 mm by 40 mm. The atrium contained four tunnels to represent pulmonary vein ostia (PVOs). The instrument was designed from a 3 mm diameter section of catheter tubing with an EM sensor mounted inside the tip. It closely resembled the dimension and echogenic properties of an ablation catheter tooltip. The tooltip was manually moved to various positions around the PVOs while the US catheter system tracked it. Fig. 18 (top) shows the experiment setup and plots the imaging plane as it followed the tooltip in four example data points. The green circles represent tooltip positions (t_1, t_2, t_3, t_4) that were randomly chosen. The lines show a top-down view of imaging planes as they intersect

the starting angle of the imager and the darkest green represents the final angle. The control inputs which led to accurate positioning and angular adjustments are shown in Fig. 17, once again demonstrating the difficulty in manually achieving this type of motion. This sweeping test was repeated ten times in varying regions of the workspace in different directions. The

This article has been accepted for inclusion in a future issue of this journal. Content is final as presented, with the exception of pagination.

LOSCHAK *et al.*: ALGORITHMS FOR AUTOMATICALLY POINTING ULTRASOUND IMAGING CATHETERS

9

Fig. 20.   Results of 3-D pointing tests (green vectors represent the imaging plane pointing at the target).

Fig. 18.   (top) Photo of tracking the instrument tip and example results from four trials. Lines show imaging plane vectors intersecting ablation tooltip positions represented by circles. Targets are within ± 1 mm of the imaging plane centerline, thus appearing in the images. (bottom) Additional instrument tracking results based on EM-reported angle errors.
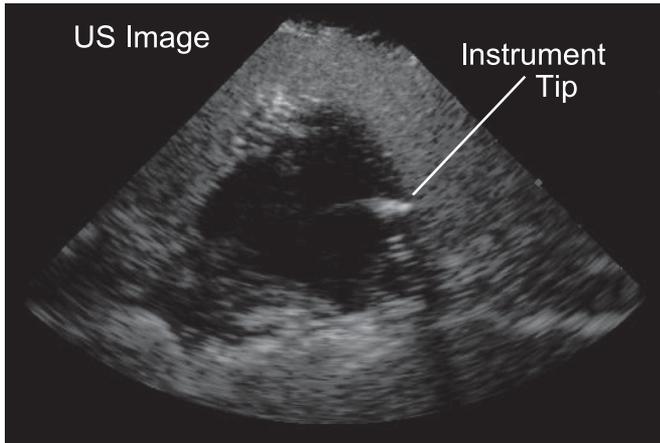
Fig. 19.   US image of instrument tip during instrument tracking.

with the tooltip. The black circle represents a cross section of the tip of the US catheter. It can be seen that the targets are within ± 1 mm of the imaging plane centerline. A larger dataset of instrument tracking test results is shown in Fig. 18 (bottom), where the angular tracking accuracy was rms $0.3°$. The US imaging plane has a non-zero thickness, that enables the instrument tip to remain visible even though the instrument tip is ± 1 mm away from the US imager centerline, as seen in Fig. 19.

D. Imager 3-D Positioning

The imager 3-D positioning and pointing algorithm was used to traverse a half-circle around a virtual target while imaging it from a fixed distance. The target could be user-defined or measured by EM sensor. Experimental results are shown in Fig. 20. Blue dots represent the location of the US imager at each position around the half-circle. The green lines represent a vector in the imaging plane which was adjusted by the robot system to point at the target. The robot reached its commanded positions with 1.6 mm rms error and pointed the imager at the object with $0.17°$ RMS error. Since cardiac anatomy poses many constraints on catheter motion, in practice, it is expected that small sections of curvature (rather than large regions of the solution set) may be useful for imaging cardiac structures from multiple angles.

VI. DISCUSSION

The robotic system for automatic steering of US imaging catheters is able to interface directly with US catheters which are already approved by regulatory organizations and have been clinically implemented for over a decade. This improves clinical feasibility and integration with existing clinical practices at the cost of requiring a greater control effort to overcome non-linearities in catheter steering. US catheter steering accuracy suffers from pull wire friction, backlash in handle knobs, and polymer effects. The results of the validation studies demonstrated accurate positioning and imager spinning capabilities of the system. This enables clinicians to move the US catheter to a safe location and image structures that are difficult to focus on by manual manipulation. Imager spinning is useful for reconstructing volumes, performing diagnoses, or lesion assessment during ablation. Imager spinning in conjunction with instrument tracking enables monitoring instrument-tissue interactions during procedures. The system also demonstrated imaging a virtual target from multiple sides. This approach can enable other visualization strategies, such as allowing a user to choose from a set of possible viewing angles.

This article has been accepted for inclusion in a future issue of this journal. Content is final as presented, with the exception of pagination.

10

IEEE TRANSACTIONS ON ROBOTICS

Throughout trials, the tip of the catheter was navigated to the desired position within the 2 mm allowable error threshold and the US imager was rotated to point at targets with sub-degree error. Position control tests were done with ≤ 1 mm/s speeds. Imager angle tests were done at $\leq 0.5°$/s. These speeds are not sufficient for accurate navigation *in vivo*. Navigational speed was not a focus of this investigation, but it will be closely examined in future work.

Steering algorithms were validated in a simulated bench top (or water tank) environment with a fixation mechanism constraining the distal bending section of the catheter. By constraining the distal section, the isolated bending motion could be studied thoroughly. Future work in algorithm design aims to improve the robustness of the controller for navigating the catheter when the distal section is less constrained. This will be necessary for *in vivo* studies in which the body of the catheter is loosely constrained throughout the vasculature. Safety boundaries inside the heart may be constructed with known locations of delicate cardiac structures (i.e., valve leaflets). Additionally, a new design for the robot with quick catheter installation and release is needed in order to conduct *in vivo* studies.

The algorithms developed for this system are useful for any long, thin, flexible tools that rely on achieving a specific orientation with respect to the target in order to complete a task. While this system was developed for use with cardiac catheters, the steering algorithms are applicable to other long flexible manipulators in other organ systems or industrial uses as well.

VII. CONCLUSION

US catheters are currently limited in clinical usage due to difficulty in manually steering the US imager in joint space. Therefore, controlling the position and orientation of the catheter tip and the imaging plane is essential for improving current catheter-based procedures and enabling additional procedures to be performed minimally invasively. The tests described in this study represent the first examples known to the authors of applying US catheter position and orientation kinematics toward robotically enhanced visualization.

With the incorporation of real time US visualization and image processing, the robot will be able to process images of cardiac structures and use inverse kinematics to navigate the catheter tip and imaging plane while maintaining specific relationships with other objects in the heart. Robotic control of US catheters has the potential to shorten procedure times, improve patient outcomes, and reduce the training time required to master use.

REFERENCES

[1] M. Moscucci, *Grossman & Baim's Cardiac Catheterization, Angiography, and Intervention*. Philadelphia, PA, USA: Lippincott Williams & Wilkins, 2013.

[2] M. Jongbloed *et al.*, "Radiofrequency catheter ablation of paroxysmal atrial fibrillation; guidance by intracardiac echocardiography and integration with other imaging techniques," *Eur. J. Echocardiography*, vol. 4, no. 1, pp. 54–58, 2003.

[3] Catheter Robotics, Inc., *Amigo Remote Catheter System*. [Online]. Available: http://catheterrobotics.com/images/AmigoBrochure.pdf, Accessed 2016.

[4] Corindus, Inc., *CorPath Robotic PCI*. [Online]. Available: http://www.corindus.com/, Accessed 2016.

[5] Hansen Medical, Inc., *Sensei X Robotic Catheter System*. [Online]. Available: http://hansenmedical.com, Accessed 2016.

[6] A. B. Koolwal, F. Barbagli, C. R. Carlson, and D. H. Liang, "A fast slam approach to freehand 3-d ultrasound reconstruction for catheter ablation guidance in the left atrium," *Ultrasound Med. Biol.*, vol. 37, no. 12, pp. 2037–2054, 2011.

[7] Stereotaxis, *Niobe ES*. [Online]. Available: http://www.stereotaxis.com/products/niobe/, Accessed 2016.

[8] Stereotaxis, *V-Drive Robotic Navigation System*. [Online]. Available: http://www.stereotaxis.com/products/vdrive/, Accessed 2016.

[9] F. M. Creighton IV, R. C. Ritter, R. R. Viswanathan, N. Kastelein, J. M. Garibaldi, and W. Flickinger, "Operation of a remote medical navigation system using ultrasound image," US Patent App. 12/205,137, Sep. 5, 2008.

[10] P. Loschak, L. Brattain, and R. Howe, "Automated pointing of cardiac imaging catheters," in *Proc. 2013 IEEE Int' Conf. Robot. Autom.*, May 2013, pp. 5794–5799.

[11] P. M. Loschak, L. J. Brattain, and R. D. Howe, "Algorithms for automated pointing of cardiac imaging catheters," in *Proc. Int. Workshop Comput.-Assisted Robot. Endoscopy*, 2014, pp. 99–109.

[12] D. B. Camarillo, C. R. Carlson, and J. K. Salisbury, "Configuration tracking for continuum manipulators with coupled tendon drive," *IEEE Trans. Robot.*, vol. 25, no. 4, pp. 798–808, Aug. 2009.

[13] R. S. Penning, J. Jung, J. Borgstadt, N. J. Ferrier, and M. R. Zinn, "Towards closed loop control of a continuum robotic manipulator for medical applications," in *Proc. 2011 IEEE Int. Conf. Robot. Autom.*, 2011, pp. 4822–4827.

[14] B. Conrad and M. Zinn, "Closed loop task space control of an interleaved continuum-rigid manipulator," in *Proc. 2015 IEEE Int. Conf. Robot. Autom.*, 2015, pp. 1743–1750.

[15] Y. Ganji, F. Janabi-Sharifi, and A. N. Cheema, "Robot-assisted catheter manipulation for intracardiac navigation," *Int J. Comput. Assisted Radiol. Surgery*, vol. 4, no. 4, pp. 307–315, 2009.

[16] I. Gravagne, C. D. Rahn, and I. D. Walker, "Large deflection dynamics and control for planar continuum robots," *IEEE/ASME Trans. Mechatron.*, vol. 8, no. 2, pp. 299–307, Jun. 2003.

[17] D. C. Rucker and R. J. Webster, "Statics and dynamics of continuum robots with general tendon routing and external loading," *IEEE Trans. Robot.*, vol. 27, no. 6, pp. 1033–1044, Dec. 2011.

[18] M. C. Yip and D. B. Camarillo, "Model-less feedback control of continuum manipulators in constrained environments," *IEEE Trans. Robot.*, vol. 30, no. 4, pp. 880–889, Aug. 2014.

[19] R. J. Webster and B. A. Jones, "Design and kinematic modeling of constant curvature continuum robots: A review," *Int. J. Robot. Res.*, vol. 29, pp. 1661–1683, 2010.

[20] J. S. Robert, *Fundamentals of robotics: Analysis and control*. New Delhi, India: Prentice-Hall, 1992, pp. 38–40.

[21] R. O. Bude and R. S. Adler, "An easily made, low-cost, tissue-like ultrasound phantom material," *J. Clinical Ultrasound*, vol. 23, no. 4, pp. 271–273, 1995.

Paul M. Loschak (S'16) received the B.S. degree in mechanical engineering from University of Florida, Gainesville, FL, USA, in 2009 and the Ph.D. degree in engineering sciences from Harvard University, Cambridge, MA, USA, in 2016.

He is a Postdoctoral Researcher at the Harvard Paulson A. School of Engineering and Applied Sciences, Cambridge, MA, USA, where his research interests include robotic systems and devices for cardiac catheterization.

This article has been accepted for inclusion in a future issue of this journal. Content is final as presented, with the exception of pagination.

LOSCHAK *et al.*: ALGORITHMS FOR AUTOMATICALLY POINTING ULTRASOUND IMAGING CATHETERS
11

Laura J. Brattain (M'14) received the Ph.D. degree in engineering sciences from Harvard University, Cambridge, MA, USA, in 2014.

She is a Technical Staff Member at the Bioengineering Systems and Technologies Group, MIT Lincoln Laboratory, Lexington, MA, USA, where her research interests include biomedical image processing and visualization, multimodal data analytics, and high performance computing.

Robert D. Howe (F'12) received the Bachelor's degree in physics from Reed College, Portland, OR, USA, and the Master's and Doctoral degrees in mechanical engineering from Stanford University, Stanford, CA, USA.

He is the Abbott and James Lawrence Professor of engineering and the Area Dean for bioengineering in the Harvard Paulson School of Engineering and Applied Sciences, Cambridge, MA, USA. He was with the electronics industry in Silicon Valley. In 1990, he joined the faculty at Harvard, where he founded the BioRobotics Laboratory, which investigates the roles of sensing and mechanical design in motor control, in both humans and robots. His research interests include manipulation, the sense of touch, haptic interfaces, and robot-assisted and image-guided surgery.